JACC: BASIC TO TRANSLATIONAL SCIENCE VOL. 3, NO. 5, 2018

PRECLINICAL RESEARCH

Novel Mechanistic Roles for Ankyrin-G in Cardiac Remodeling and Heart Failure

Michael A. Makara, PhD,[a,b] Jerry Curran, PhD,[a,b] Ellen R. Lubbers, BS,[a,b] Nathaniel P. Murphy, BS,[a,b] Sean C. Little, PhD,[a,b] Hassan Musa, PhD,[a,b] Sakima A. Smith, MD,[a,b,c] Sathya D. Unudurthi, PhD,[a,d] Murugesan V.S. Rajaram, PhD,[a,e] Paul M.L. Janssen, PhD,[a,b] Penelope A. Boyden, PhD,[f] Elisa A. Bradley, MD,[a,c] Thomas J. Hund, PhD,[a,d] Peter J. Mohler, PhD[a,b,c]

VISUAL ABSTRACT

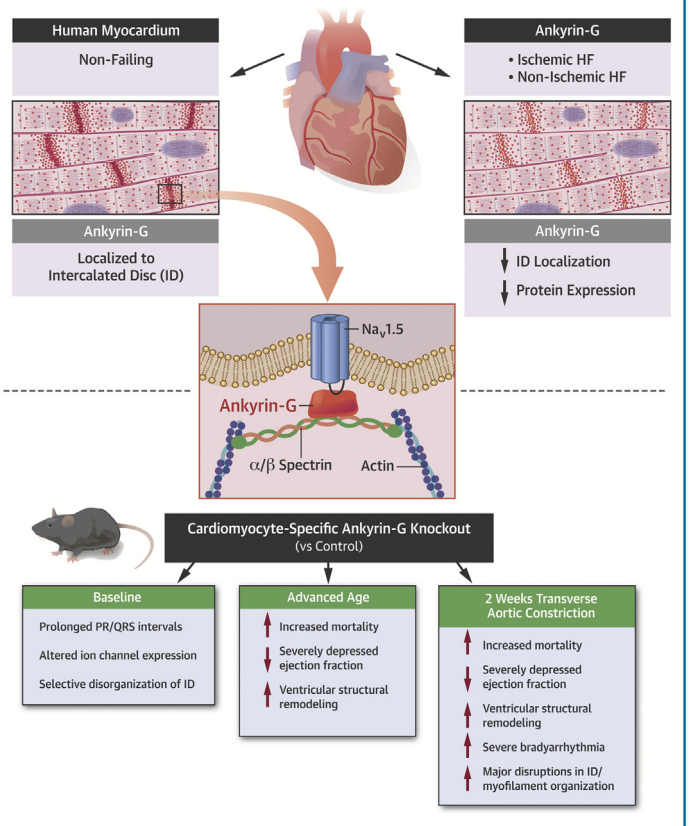

Makara, M.A. et al. J Am Coll Cardiol Basic Trans Science. 2018;3(5):675–89.

HIGHLIGHTS

- **The pathogenesis of human heart failure is complex, and the creation of new therapeutic strategies for human heart failure is critical.**
- **Identifying the molecular pathways underlying heart failure is important to define potential new therapeutic targets.**
- **Ankyrin polypeptides serve to target and stabilize membrane proteins in cardiomyocytes.**
- **Ankyrin-G levels are altered in humans and mice with heart failure, and mice lacking ankyrin-G in cardiomyocytes develop cardiomyopathy and systolic dysfunction.**
- **Mechanistically, ankyrin-G is necessary for the expression and localization of critical myocyte proteins essential for regulating cardiac structural and electrical activity.**

From the [a]Dorothy M. Davis Heart & Lung Research Institute, The Ohio State University Wexner Medical Center and College of Medicine, Columbus, Ohio; [b]Department of Physiology and Cell Biology, The Ohio State University Wexner Medical Center and College of Medicine, Columbus, Ohio; [c]Department of Internal Medicine, The Ohio State University Wexner Medical Center and College of Medicine, Columbus, Ohio; [d]Department of Biomedical Engineering, The Ohio State University College of Engineering, Columbus, Ohio; [e]Department of Microbial Infection and Immunity, Center for Microbial Interface Biology, The Ohio State University College of Engineering, Columbus, Ohio; and the [f]Department of Pharmacology, Columbia University, New York, New York. This work is supported by the Ohio State JB Project and Healing Hearts of Central Ohio. The authors are supported by NIH

ISSN 2452-302X https://doi.org/10.1016/j.jacbts.2018.07.008

JACC: BASIC TO TRANSLATIONAL SCIENCE VOL. 3, NO. 5, 2018
OCTOBER 2018:675–89

ABBREVIATIONS AND ACRONYMS

AnkG = ankyrin-G

cKO = cardiomyocyte-specific knockout

DSP = desmoplakin

ECG = electrocardiogram

HF = heart failure

LV = left ventricular

PBS = phosphate-buffered saline

PKP2 = plakophilin-2

TAC = transverse aortic constriction

TUNEL = terminal deoxynucleotidyl transferase dUTP nick-end labeling

WT = wild-type

SUMMARY

Ankyrin polypeptides are intracellular proteins responsible for targeting cardiac membrane proteins. Here, the authors demonstrate that ankyrin-G plays an unexpected role in normal compensatory physiological remodeling in response to myocardial stress and aging; the authors implicate disruption of ankyrin-G in human heart failure. Mechanistically, the authors illustrate that ankyrin-G serves as a key nodal protein required for cardiac myofilament integration with the intercalated disc. Their data define novel in vivo mechanistic roles for ankyrin-G, implicate ankyrin-G as necessary for compensatory cardiac physiological remodeling under stress, and implicate disruption of ankyrin-G in the development and progression of human heart failure. (J Am Coll Cardiol Basic Trans Science 2018;3:675–89)

Maintenance of left ventricular (LV) systolic function requires the coordinated conduction of action potentials between cardiomyocytes in concert with sufficient transmission of force from cell to cell. To accomplish this, cardiomyocytes are coupled both electrically and mechanically at their terminal ends by a specialized membrane structure known as the intercalated disc (1). At the intercalated disc, gap junctions electrically couple adjacent cells, acting as low resistance pathways to propagate action potentials between cardiomyocytes (2). The fascia adherens junction and the desmosome, integrating the plasma membrane with actin and intermediate filaments, respectively, provide mechanical coupling (3,4). In both acquired and congenital heart disease, defects in these intracellular structures contribute to systolic dysfunction and heart failure (HF) (3–5). Therefore, elucidating the molecular pathways responsible for the maintenance of mechanical and electrical coupling of cardiomyocytes is critical to gain insight into the pathogenesis of human HF.

Ankyrin polypeptides (ankyrin-R, ankyrin-B, and ankyrin-G [AnkG]) are intracellular scaffolding proteins responsible for targeting cellular membrane proteins, regulating both cellular excitability and structure. Ankyrin-B (*ANK2*) is tightly linked with the expression and targeting of critical membrane, structural, and signaling proteins. Ankyrin-B dysfunction is linked with both congenital and acquired forms of human arrhythmia and HF (6–16). By contrast, cardiac AnkG (*ANK3*) is less studied, yet closely linked with arrhythmia phenotypes in both humans and animal models through its association with the voltage-gated Na_v channel, $Na_v1.5$ (*SCN5A*). Human *SCN5A* variants that have an impact on AnkG/$Na_v1.5$ interactions are associated with Brugada syndrome (17); myocytes and mice lacking cardiac AnkG display altered conduction and arrhythmia phenotypes (18–20); and large animal models of cardiovascular disease display altered AnkG and $Na_v1.5$ pathways (21). Recently, new roles for AnkG beyond regulating cardiac excitability have emerged. For example, the interaction of AnkG with plakophilin-2 (*PKP2*) (22) supports a potential role in both myocyte electrical function (via $Na_v1.5$) and in cardiac mechanical coupling. However, the in vivo functional role that AnkG plays in regulating mechanical coupling of cardiomyocytes (baseline and in disease) is unknown and untested.

Here, we identify an unexpected requirement of cardiac AnkG for normal cardiac structure and function. We illustrate in both humans and mice a striking change in AnkG levels during key stages of cardiac remodeling both in compensatory hypertrophy and in end-stage dilated cardiomyopathy. Moreover, the key role of AnkG in cardiac remodeling is supported by studies in mice lacking cardiac AnkG expression.

grants HL135754, HL134824, HL139348, HL135096, and HL114383 (Dr. Mohler), HL135437 (Dr. Smith), HL135096, HL134824, and HL114893 (Dr. Hund), HL137331 (Ms. Lubbers), and HL137325 (Mr. Murphy). Dr. Makara has been employed by DOCS Global (CRO) as a medical writer contracting for Merck Sharpe & Dohme Corp. Dr. Curran has been an employee of Abiomed. Dr. Little has been employed by Bristol-Myers Squibb. All other authors have reported that they have no relationships relevant to the contents of this paper to disclose.

All authors attest they are in compliance with human studies committees and animal welfare regulations of the authors' institutions and Food and Drug Administration guidelines, including patient consent where appropriate. For more information, visit the *JACC: Basic to Translational Science* author instructions page.

Manuscript received April 3, 2018; revised manuscript received July 5, 2018, accepted July 31, 2018.

Specifically, we demonstrate that mice lacking AnkG expression in cardiac myocytes develop dilated cardiomyopathy and severe systolic dysfunction with age. Further, in a transverse aortic constriction (TAC) model, where afterload is increased, AnkG cardiomyocyte-specific knockout (cKO) animals display increased mortality mediated by severe systolic dysfunction. Mechanistically, we illustrate that AnkG serves as a key nodal protein required for cardiac myofilament integration with the intercalated disc. We show that AnkG is required for normal expression and/or distribution of a select group of myocyte disc proteins including plakophilin-2 (PKP2), desmoplakin (DSP), desmin, and $Na_v1.5$. Together, our data demonstrate that AnkG is necessary to maintain normal cardiac structure and function at baseline and in response to chronic stress, and implicate disruption of AnkG as playing a central role in the development and progression of human HF.

METHODS

HUMAN HEART TISSUE. Failing (ischemic/nonischemic) LV tissue was obtained from explanted hearts undergoing heart transplantation through The Cooperative Human Tissue Network: Midwestern Division at The Ohio State University. Nonfailing hearts were obtained through an approved relationship with Lifeline of Ohio. The local institutional review board provided approval for the use of human subject tissue. Age and sex were the only identifying information collected from the medical record. This investigation conforms with the principles outlined in the Declaration of Helsinki.

IMMUNOFLUORESCENCE. Cardiomyocytes (left ventricle) and cryosections (5-μm thickness) were isolated/prepared from control and cKO (baseline/TAC) hearts as follows (23). Isolated cells and tissue slices were fixed and permeabilized in 100% ethanol at −20°C. Cells/sections were blocked in 3% fish skin gelatin and 0.1% Triton X-100 in phosphate-buffered saline (PBS). Cells/sections were incubated with primary antibody overnight in blocking solution. Cells/sections were stained with secondary antibodies in blocking solution for >1 h at room temperature. Secondary antibodies included Alexa-conjugated donkey anti-mouse 488, 568, and donkey anti-rabbit 488, 568. Cells/sections were analyzed on a LSM 780 confocal microscope (24) (Carl Zeiss, Oberkochen, Germany). Cells/sections were imaged using identical confocal settings between genotypes.

IMMUNOBLOTTING AND ANTIBODIES. Human ventricular and murine whole-heart lysates, following quantitation by BCA assay (Pierce, Thermo Fisher Scientific, Waltham, Massachusetts), were loaded into 4% to 15% pre-cast gels (Bio-Rad Laboratories, Hercules, California) and transferred to nitrocellulose membranes (25). Membranes were blocked for >1 h at room temperature in 5% milk and incubated in primary antibody overnight at 4°C. Primary antibodies included AnkG (1:1,000, Santa Cruz Biotechnology, Dallas, Texas), N-cadherin (1:2,000; Invitrogen, Carlsbad, California), PKP2 (1:500, isolated cells; Abcam, Cambridge, United Kingdom), PKP2 (undiluted, cryoslices; American Research Products, Waltham, Massachusetts), GAPDH (1:5,000, Fitzgerald Industries International, Acton, Massachusetts). Secondary antibodies used were donkey anti-mouse-HRP and donkey anti-rabbit-HRP (1:5,000, Jackson ImmunoResearch Laboratories, West Grove, Pennsylvania). Densitometric analysis was performed using Image Lab software (version 5.2.1 build 11. 2014, Bio-Rad Laboratories), and all protein expression data were normalized to GAPDH expression. In multiple cases, GAPDH is same as blots were either cut or reprobed using unique antibodies for primary probe.

TRANSVERSE AORTIC CONSTRICTION. To produce pressure overload (increased afterload) conditions, TAC was performed on 8-week-old mice. Briefly, mice were anesthetized with isoflurane (2.5%) and intubated. Intubated mice were placed on a respirator (120 breaths/min, 0.1-ml tidal volume), and anesthesia was maintained throughout the procedure. The thoracic cavity was opened using a partial midline sternotomy, and the transverse aorta was exposed via blunt dissection. Once the aorta was identified, a 6.0 Prolene suture was placed around the transverse aorta between the brachiocephalic and left common carotid artery. The suture was tightened around a 27-ga needle and placed next to the aorta to standardize the degree of constriction. The needle was then removed, the thoracic cavity and overlying skin was closed, and appropriate analgesia was administered (buprenorphine 0.1 mg/kg, intraperitoneally). For sham control subjects (age/sex matched), the identical protocol was used without the aortic constriction. At termination of experiments (2 weeks post-TAC/sham surgery), mice were anesthetized (2% tribromoethanol, 20 μl/g body weight, intraperitoneally) and sacrificed via thoracotomy. Following euthanasia of the animals, the heart, lung, and tibia were removed for analysis. We did not witness any death in sham-operated animals (animals that underwent the identical surgical procedure as the animals receiving TAC). Furthermore, per our standard laboratory procedure, any mouse that died within 1 to 3 days (any mouse where death could be linked to the surgical procedure) is excluded from the dataset.

TELEMETRY. Following TAC/sham surgery, mice had ETA-F10 radiotelemeters implanted (DSI PhysioTel, Data Sciences International St. Paul, Minnesota). Following surgery, mice recovered for 7 days before electrocardiogram (ECG) recordings. Average resting heart rates (sham/TAC) were obtained from continuous 2-h ECG recordings at 2 weeks post-surgery. ECG tracings and waveforms were analyzed using P3 Plus software (Ponemah version 5.20, Data Sciences International).

ANIMALS. Mice lacking AnkG in adult cardiac myocytes (αMHC-Cre x ankyrin-$G^{f/f}$; cKO) mice were engineered by crossing ankyrin-$G^{f/f}$ (LoxP sites flanking exons 22 to 23 of *Ank3* and NEO cassette already removed from line [18]) with mice expressing Cre under the cardiac promoter α-myosin heavy chain (αMHC-Cre). Wild-type (control) and AnkG cKO male mice were used (8 weeks of age at the start of the experiment, C57/Bl6 background). All animal studies and surgeries were performed in accordance with the American Physiological Society Guiding Principles for Research Involving Animals and Human Beings and approved by the Ohio State University Institutional Animal Care and Use Committee. The investigation conforms to the Guide for the Care and Use of Laboratory Animals published by the NIH (Publication No. 85-23, revised 1996).

ECHOCARDIOGRAPHY. Two-dimensional echocardiography (Vevo 2100, FUJIFILM VisualSonics, Toronto, Ontario, Canada) was performed before surgery and at 2 weeks following surgery. Using a MS-400 18- to 38-mHz cardiovascular transducer, parasternal long-axis images were obtained to confirm orientation of the heart. Once confirmed, short-axis images at the level of the papillary muscles were obtained, and M-mode was applied. M-mode was used to determine chamber size and function including: LV anterior wall end-diastolic dimension, posterior wall end-diastolic dimension, LV cavity end-diastolic dimension, and LV cavity end-systolic dimension. Functional data were derived from the M-mode measurements, including fractional shortening and ejection fraction.

HISTOLOGY. Hearts were explanted and fixed in 10% formalin, processed, and then embedded into paraffin for sectioning. Hearts were sectioned along the long axis (4-chamber view) at a thickness of 10 μm. Sections were stained with hematoxylin and eosin to examine general structure and histology, and with Masson's trichrome to visualize collagen deposition (fibrosis).

TUNEL STAINING. Paraffin-embedded heart sections were deparaffinized with xylene followed by rehydration with graded alcohols (100%, 95%). A heat-induced epitope retrieval procedure was carried out by heating the tissue slides in citrate buffer (pH 6.0) at 95°C for 10 min. Each tissue section was rehydrated with PBS, blocked (5% nonfat dry milk in PBS + 0.01% sodium azide) for 3 h at room temperature and subjected to a terminal deoxynucleotidyl transferase dUTP nick end labeling (TUNEL) assay. Apoptotic cells were stained by the Click-iT Plus TUNEL assay for in situ apoptosis detection and Alexa Fluor 488 dye from Molecular Probes Life Technology (Thermo Fisher Scientific). The nuclei were stained with Hoechst 33342 solution and examined under confocal microscopy (26). Ten random images were taken from each heart ($n = 3$), and total nuclei and TUNEL-positive nuclei were quantified. Data are represented as percent TUNEL-positive nuclei total nuclei ± SEM.

TRANSCRIPT ANALYSIS. Total RNA was isolated from the hearts of 3- to 4-month-old wild-type (WT) and AnkG cKO mice using the Qiagen RNeasy Mini Kit per manufacturer instructions (QIAGEN, Valencia, California). Relative transcript expression levels were determined using the GeneChip Mouse Gene 2.0 ST Array (Affymetrix, Santa Clara, California). Following quality assessment and background error correction, low-expression genes were filtered from the dataset (9,736 genes remaining of 26,688 genes in total). A moderated Student's *t*-test was applied to the small sample comparison to stabilize the variance of genes and degree of freedom. Further, the mean number of false positives was used to determine the significance threshold for the p values.

STATISTICS. Data were analyzed using SigmaPlot Version 12.0 (Systat Software, San Jose, California). The p values were determined with the unpaired Student's *t*-test (2 tailed) in the case of single comparisons and with 1-way analysis of variance in the case of multiple comparisons. The Newman-Keuls multiple comparison test was used for post hoc testing. If the data distribution failed normality tests with the Shapiro-Wilk test, rank-based analysis of variance and the Dunn multiple-comparisons test were performed. Incidence of death following bradyarrhythmia was analyzed by the chi square test. Kaplan-Meier survival analysis was used to determine risk of mortality during aging, as well as following the TAC procedure. In all cases, a p value < 0.05 was considered statistically significant.

RESULTS

AnkG EXPRESSION IS ALTERED IN HUMAN HF. Several reports have documented dysregulated

FIGURE 1 AnkG Expression Is Reduced in Human HF

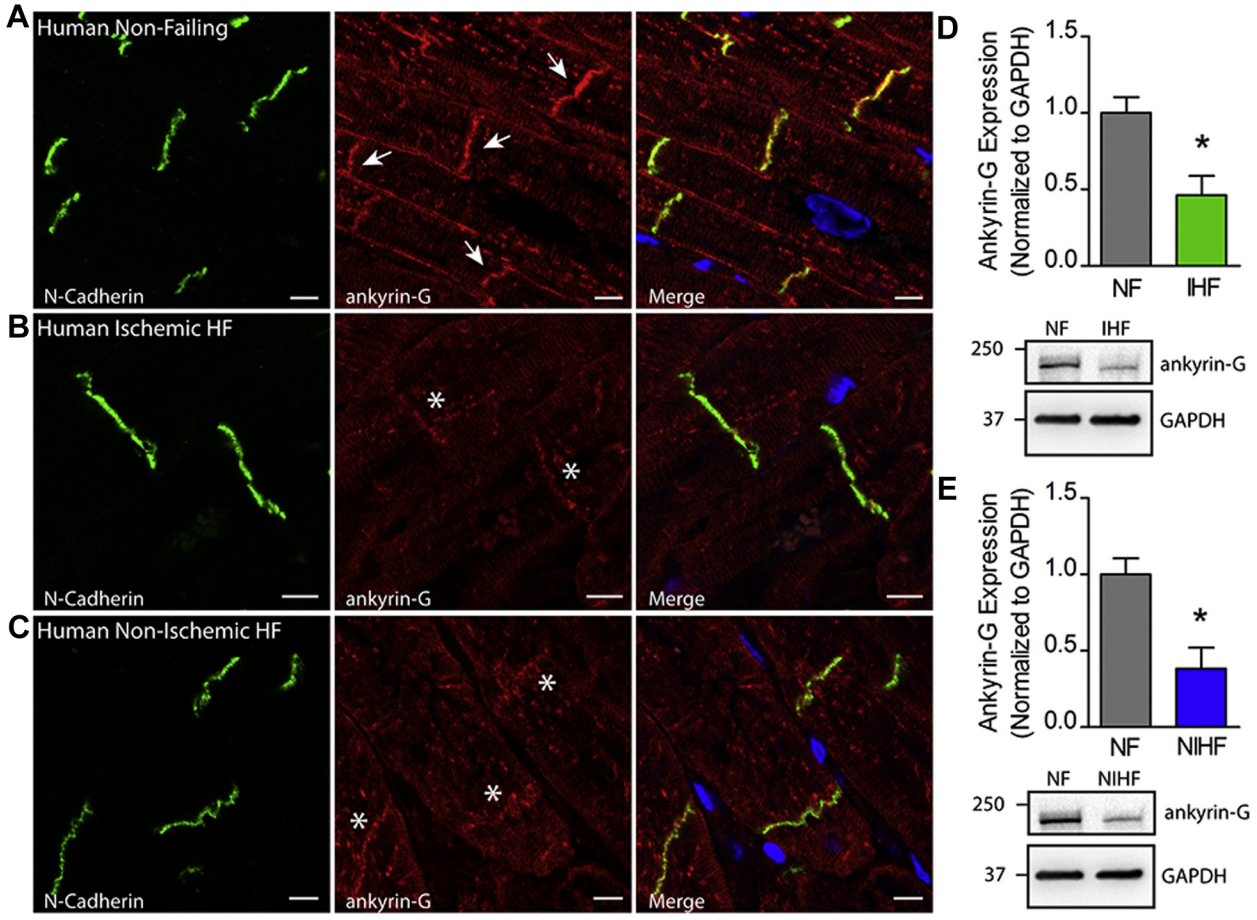

N-cadherin **(green)** and AnkG staining **(red)** in the left ventricle of **(A)** non-failing human heart, as well as hearts from individuals with **(B)** ischemic HF and **(C)** nonischemic HF. In **A**, **arrows** note strong localization of AnkG at the intercalated disc. In **B and C**, **asterisks** denote AnkG loss. Nuclei are visualized in **blue** (bar = 10 μm). Immunoblot analysis demonstrates a decrease in total AnkG expression in **(D)** ischemic and **(E)** nonischemic heart failure compared with nonfailing hearts (n = 3 NF; n = 5 IHF; n = 5 NIHF; $p < 0.05$). AnkG = ankyrin-G; HF = heart failure; IHF = ischemic heart failure; NF = nonfailing; NIHF = nonischemic heart failure.

expression of AnkG in noncardiac pathophysiology, including generalized ischemia (27) and traumatic brain injury (28). On the basis of these data, we investigated the regulation of AnkG in the setting of human HF. Immunostaining of nonfailing human heart tissue demonstrated predominant localization of AnkG to the intercalated disc (Figure 1A). In both ischemic and nonischemic human HF (Figures 1B and 1C), AnkG expression at the intercalated disc was significantly reduced. Similarly, immunoblot analysis demonstrated a significant reduction (~50%) of AnkG expression in the left ventricle of both ischemic and nonischemic human HF tissue relative to nonfailing control samples (Figures 1D and 1E). Thus, AnkG expression is altered in human HF.

AnkG LEVELS ARE ALTERED IN CARDIAC HYPERTROPHY AND HF IN MICE. To explore the temporal expression profile of AnkG during chronic stress (as opposed to end-stage HF as in the case of human data), we investigated the relationship of AnkG expression during the acute and chronic stages of cardiac remodeling in response to the acute afterload increase induced by TAC. In C57Bl/6J mice, this procedure generally produces LV hypertrophy at ~1 week and cardiac decompensation at approximately 6 weeks (29-31). We observed an unexpected increase in 190-kD AnkG (primary cardiac isoform) expression in WT hearts 2 weeks following TAC (Figures 2A and 2C) (~2.25 fold; $p < 0.05$), a time point during which the heart is actively undergoing compensatory

FIGURE 2 AnkG Levels Are Altered During Pressure Overload-Induced Cardiac Remodeling and HF

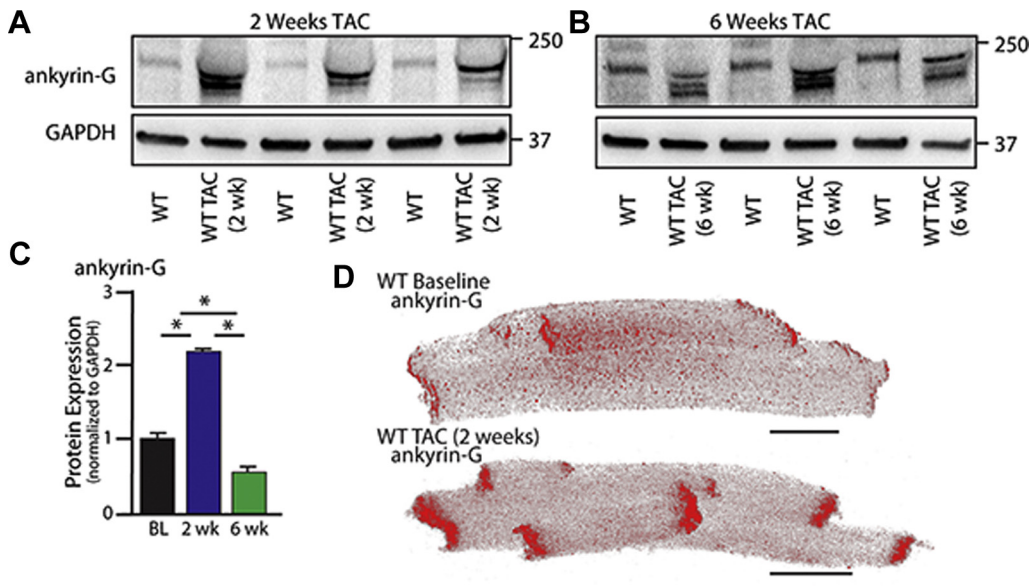

(A and C) 190-kDa ankyrin-G (AnkG) protein expression levels are significantly increased in wild-type (WT) mouse hearts following 2 weeks transverse aortic constriction (TAC) ($n = 3$ for both groups; $p < 0.05$). **(B and C)** AnkG protein levels are significantly reduced in WT mouse hearts following 6 weeks TAC ($n = 3$ for both groups; $p < 0.05$). In **C**, densitometry was performed of full-length, mature, 190-kD AnkG (vs. lower molecular weight products). **(D)** AnkG immunostaining (3-dimensional composite of Z-stacks) in WT myocytes at baseline (BL) and 2 weeks post-TAC visualized using a ratiometric filter to compare intensity. Note the striking increase in AnkG expression at the intercalated disc of the 2-week TAC myocyte. Scale bars = 20 μm.

hypertrophic remodeling. By contrast (and consistent with human HF data), we observed a reduction in AnkG expression in WT mice at 6 weeks post-TAC, with multiple low molecular weight AnkG isoforms, likely representing degradation products, in all experiments (Figures 2B and 2C) ($p < 0.05$).

AnkG is primarily localized to the intercalated disc of the cardiomyocyte (Figure 2D) (18,32,33). Myocytes isolated from hearts following 2 weeks TAC demonstrate a significant up-regulation of AnkG expression at the intercalated disc compared with WT myocytes (Figures 2C and 2D). Z-stack confocal microscopy confirmed significant increases of AnkG localization at the intercalated disc after 2 weeks TAC (Figure 2D), occurring simultaneously during cardiomyocyte hypertrophy. In summary, AnkG expression is increased during compensatory hypertrophic remodeling, but reduced as animals progress to a dilated cardiomyopathy phenotype, indicating that AnkG plays a critical role in cardiac structural remodeling.

AnkG cKO MICE DISPLAY INCREASED VENTRICULAR DYSFUNCTION WITH ADVANCED AGE. To investigate the specific role of AnkG in regulating cardiac function, we generated mice lacking AnkG expression in adult cardiomyocytes (see the Methods section). At 2 months, AnkG cKO displayed normal heart structure with only a minor reduction in systolic function compared with control mice. However, beginning at 10 months, AnkG cKO mice demonstrated increased mortality. In fact, only 30% of AnkG cKO mice survived to 15 months (Figure 3A) (3 of 10 cKO vs. 10 of 10 control mice; $p < 0.05$). Aged AnkG cKO mice (12 months) displayed significant biventricular dilatation (Figures 3B, 3C, and 3E) and increased heart weight/tibia length ratio (Figure 3D) (control 10.2 ± 0.8; cKO 18.51 ± 2.5; $p < 0.05$). Surviving AnkG cKO mice at 12 months demonstrated significantly reduced LV systolic function (Figures 3E and 3F) (WT $50 \pm 2\%$; cKO $31 \pm 7\%$; $p < 0.05$; additional parameters in Figures 3G to 3I). Finally, AnkG cKO, but not WT, mice displayed significant myocardial fibrosis and vacuolization (34,35) not seen in control mice (Figures 3J and 3K). These data support an unexpected requirement of AnkG in normal cardiac structure and function with AnkG deficiency leading to spontaneous biventricular dilatation and HF with advanced age, as well as premature death.

AnkG LOSS ACCELERATES CARDIAC REMODELING AND MORTALITY FOLLOWING PATHOLOGICAL STRESS. The relationship between AnkG and cardiac dysfunction is primarily limited to altered

FIGURE 3 AnkG cKO Mice Display Increased Ventricular Dysfunction With Age

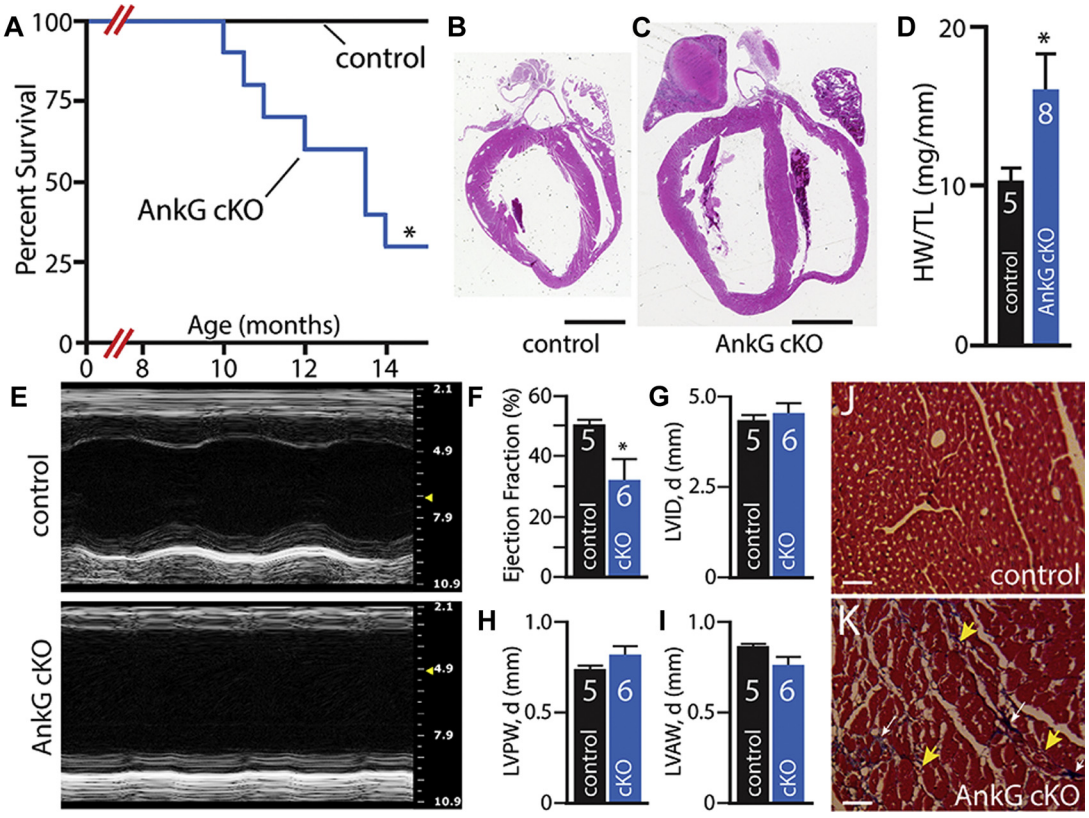

(A) Kaplan-Meier survival analysis demonstrates increased mortality in AnkG cKO mice beginning at 10 months of age (15-month survival: control 10 of 0; AnkG cKO 3 of 10; *$p < 0.05$). **(B and C)** Hematoxylin and eosin staining of control and AnkG cKO hearts demonstrate enlarged hearts with increased heart weight to tibia length ratio (HW/TL) at 12 months of age **(D)** ($p < 0.05$). **(E and F)** M-mode images of control and AnkG cKO hearts demonstrate a significant decrease in ejection fraction in AnkG cKO mice at 12 months ($p < 0.05$). Imaging illustrates unchanged **(G)** LVID,d, **(H)** LVPW,d, and **(I)** LVAW,d in AnkG cKO at 12 months of age compared with control mice. **(J and K)** Compared with age-matched control mice, 12-month AnkG cKO hearts display fibrosis and severe vacuolization (scale bars = 100 μm). AnkG = ankyrin-G; cKO = cardiomyocyte-specific knockout; LVAW,d = left ventricular anterior wall end-diastolic dimension; LVID,d = L left ventricular cavity end-diastolic dimension; LVPW,d = left ventricular posterior wall end-diastolic dimension.

electrical dysfunction, through the linkage of AnkG with the primary voltage-gated Na_v channel, $Na_v1.5$ (17-19,32). However, our new data support that AnkG is integral to normal cardiac structure and function. To test the impact of AnkG loss in the face of increased afterload leading to compensatory remodeling and eventually pathological remodeling, we analyzed AnkG cKO mice following TAC. Unlike control animals, AnkG cKO mice displayed mortality beginning 2 weeks post-TAC (**Figure 4A**) (control 1 of 8 died before 8 weeks post-surgery; cKO 8 of 14 died before 8 weeks post-surgery; $p < 0.05$). Further analysis of the post-TAC phenotype focused on mice 2 weeks post-TAC. Unlike control mice, AnkG cKO mice displayed increased heart weight/tibia length ratio and lung weight/tibia length ratio at ~2 weeks post-TAC (**Figures 4B and 4C**) ($p < 0.05$; detailed functional parameters in Supplemental Figures 1 and 2). Gross histological examination of cardiac sections (**Figures 4D to 4G**) demonstrated chamber dilation and elongation in AnkG cKO, but not control animals, after only 2 weeks following TAC.

At 8 weeks of age, we observed no difference in myocardial fibrosis in either control or AnkG cKO animals (**Figures 4H and 4I**). However, after only 2 weeks post-TAC, we observed significant myocardial remodeling, including increased fibrosis and

FIGURE 4 Severe Ventricular Remodeling in AnkG cKO Mice Following TAC

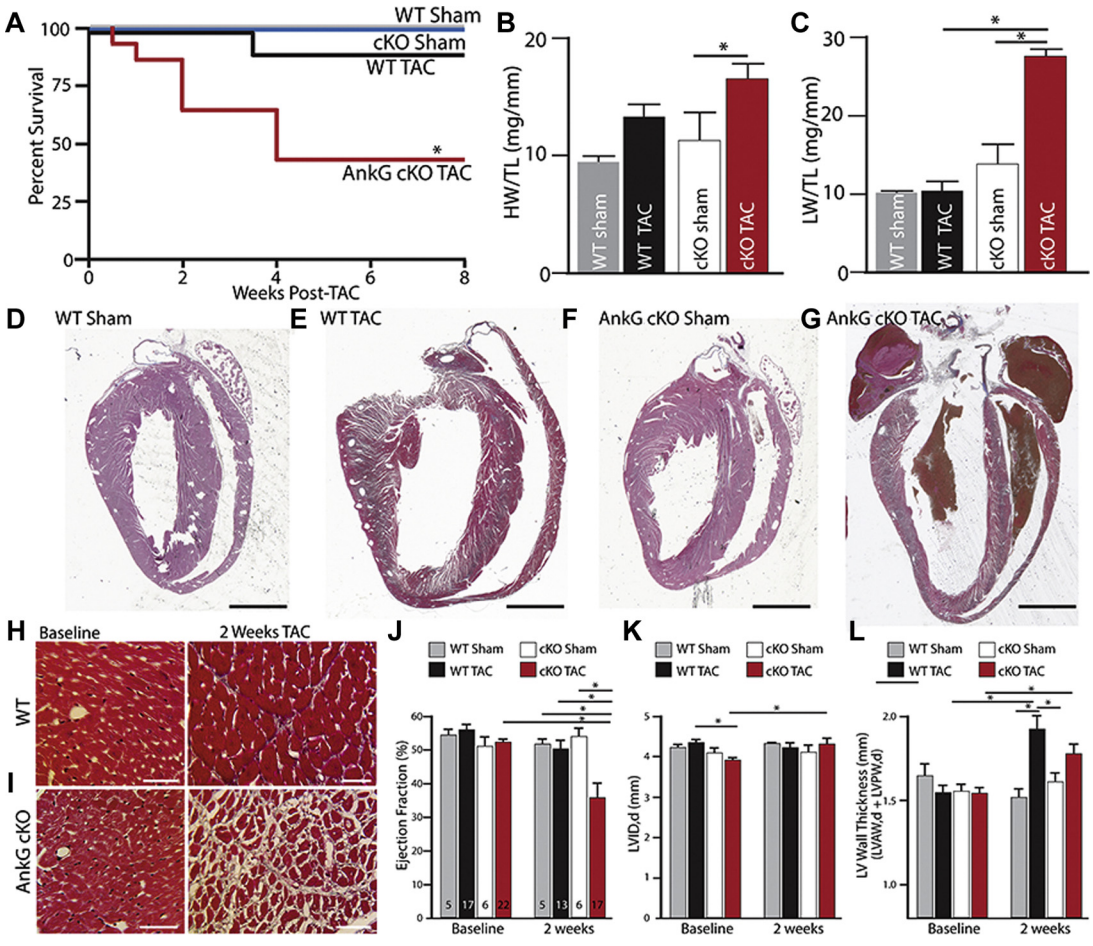

(A) Kaplan-Meier survival analysis demonstrates increased mortality in AnkG cKO mice beginning at 2 weeks post-TAC (8-week survival: control TAC 7 of 8; AnkG cKO TAC 6 of 14; control sham 5 of 5; AnkG cKO sham 6 of 6). AnkG cKO hearts demonstrate **(B)** similar heart weight to tibia length ratio compared with WT hearts at baseline with an increase in heart weight to tibia length in AnkG cKO mice at 2 weeks post-TAC ($n = 4$ control 2 weeks; $n = 5$ control 8 weeks; $n = 10$ AnkG cKO TAC). **(C)** AnkG cKO TAC hearts demonstrate a statistically significant increase in lung weight to tibia length (LW/TL) ratio at 2 weeks post-TAC ($p < 0.05$). **(D to G)** Representative sections stained with Masson's trichrome illustrate dramatic enlargement of cKO hearts following the 2-week TAC protocol. **(H and I)** Masson's trichrome staining (40× magnification) of **(H)** control (WT) and **(I)** AnkG cKO heart sections at baseline demonstrate preserved myocardial structure at baseline. WT hearts post-TAC also display preserved cardiac tissue structure **(H, right)**. By contrast, **(I, right)** AnkG cKO TAC hearts demonstrate severe vacuolization (scale bars = 50 μm). **(J to L)** Echocardiographic data for control and AnkG cKO hearts at baseline and 2 weeks post-TAC. Data include **(J)** ejection fraction, **(K)** LVID,d, and **(L)** LVPW,d and LVAW,d ($p < 0.05$; numbers are listed in the bar graph in **J**). Abbreviations as in Figures 2 and 3.

presence of vacuolization in AnkG cKO hearts, compared with control animals (**Figures 4H and 4I**). Although we observed an increase in myocyte cross-sectional area in control hearts 2 weeks post-TAC, supporting concentric hypertrophy at the cellular level, AnkG cKO hearts did not display increased cross-sectional area 2 weeks post-TAC (Supplemental Figure 3A) indicating a lack of significant concentric hypertrophy. We observed no significant difference in cell death (TUNEL-positive myocytes) between genotypes either at baseline or following the 2-week TAC protocol (Supplemental Figure 3B).

AnkG cKO mice demonstrated a severe reduction in systolic function already at 2 weeks follow-up post-TAC (**Figure 4J**). LV chamber size and systolic function were decreased in cKO mice compared with control animals at baseline (**Figures 4J to 4L**). However, at 2 weeks post-TAC, AnkG cKO animals already

displayed significant ventricular dilatation not yet observed in control mice (**Figure 4K**). Furthermore, AnkG cKO mice displayed a blunted compensatory hypertrophic change in wall thickness compared with control mice (**Figure 4L**, Supplemental Figures 1 and 2). In summary, AnkG expression appears to blunt the necessary compensatory physiological remodeling in response to increased afterload in the TAC model.

AnkG cKO MICE DISPLAY BRADYCARDIA AND BRADYARRHYTHMIAS BEFORE DEATH. As evidenced by ambulatory ECG recordings (**Figures 5A to 5D**), baseline AnkG cKO animals displayed lower resting heart rates compared with control subjects (**Figure 5E**) (control 601 ± 8 beats/min; cKO 498 ± 21 beats/min; $p < 0.05$). This trend was also true between genotypes 2 weeks post-TAC (control TAC 679 ± 17 beats/min; $p < 0.05$; cKO TAC 555 ± 17 beats/min; $p < 0.05$). At baseline, AnkG cKO animals displayed prolonged PR and QRS intervals (**Figures 5F and 5G**). Further, compared with control TAC animals at 2 months of age, AnkG cKO TAC mice displayed significantly increased PR interval length, without any significant difference in QRS interval length. Tachyarrhythmias were not the cause of mortality in AnkG cKO mice post-TAC. Ambulatory recordings of conscious AnkG cKO TAC animals at the time of death revealed a higher incidence of bradyarrhythmias preceding death (**Figures 5H and 5I**) (control 0 of 4; cKO 4 of 7; $p < 0.05$). In summary, mortality of AnkG cKO mice following TAC is linked with dilated cardiomyopathy, not tachyarrhythmia.

DEFINING NEW AnkG-ASSOCIATED PATHWAYS IN THE HEART. A role for AnkG in regulating the cardiac remodeling response to chronic stress (TAC) was unexpected. Although AnkG is known to associate with key membrane ion channels and adapter proteins (18,22,32), we analyzed differentially expressed mRNAs between control and AnkG cKO mouse LV tissue as an initial step to identify potential new pathways associated with AnkG. We performed our analysis in young mice before changes in cardiac function. From >25,000 transcripts analyzed, only a small subset of transcripts (487) displayed a corrected p value of <0.05 (**Figures 6A to 6E**) (see Supplemental Tables 1 and 2 for transcripts either up- or down-regulated between control and AnkG cKO mouse hearts). We observed differences in transcripts from ion channel subunits (**Figure 6E**) (*Scn1b, Kcnd2, Kcnv2, Kcnd2, Cacna1s, Kcnj11*), molecular motors (*Kif16b, Kif1b*), and ankyrin-associated adapters (**Figure 6D**) (*Spna1*). Interestingly, Gene Ontology Analysis (Panther [Protein Analysis Through Evolutionary Relationships] v10) identified the molecular function "cytoskeletal protein-binding" as statistically over-represented in the dataset (**Figures 6B to 6D**). Indeed, we were struck by the disproportional (>17%) transcriptional changes in cytoskeletal and cell adhesion molecules including *Dsc2* (desmocollin 2), *Ncam1* (neural cell adhesion molecule 1), *Sntb1* (β1-syntrophin), and *Ctnna3* (α-catenin) (**Figure 6D**). These data suggest that alterations in AnkG expression have an important, yet selective, impact in regulating the cardiac transcriptional program, with significant remodeling observed in the cardiac cell adhesion and cytoskeletal systems in the setting of AnkG deficiency. Further, these data support that changes in multiple ion channels, ion channel subunits, and regulatory proteins may be involved in altering both structural and electrical phenotypes in AnkG cKO heart. For example, alterations in QRS interval alone may be linked with alterations in Na^+, K^+, and Ca^{2+} channel subunits (36,37).

AnkG cKO MICE DISPLAY DEFECTS IN INTERCALATED DISC/MYOFILAMENT ORGANIZATION. On the basis of our transcriptional findings and preferential localization of AnkG at the cardiac intercalated disc, we hypothesized that AnkG expression (**Figure 7A**) was required for proper regulation of intercalated disc structural proteins at baseline and following acute increases in afterload (TAC). Although we did not observe significant differences between genotypes in desmocollin-2 expression (**Figure 7B**), DSP expression was significantly increased at baseline in AnkG cKO hearts compared with control hearts (**Figure 7C**). Further, compared with baseline, DSP levels were significantly reduced in AnkG cKO hearts following the 2-week TAC protocol (**Figure 7C**). Beyond DSP, consistent with prior findings at baseline (18,22), we observed dysregulation of PKP2 expression and cellular targeting in AnkG cKO hearts. Specifically, AnkG cKO animals demonstrate ~40% increase in PKP2 expression levels relative to control (**Figure 7D**). PKP2 expression was significantly increased in the setting of pressure overload (**Figure 7D**). However, following 2 weeks TAC, PKP2 expression in AnkG cKO hearts doubled from AnkG cKO baseline (**Figure 7D**). Further, PKP2 expression in AnkG cKO TAC animals was increased relative to WT TAC control animals (**Figure 7D**). Immunostaining revealed that unlike in control myocytes where PKP2 is enriched at the intercalated disc, PKP2 is redistributed throughout the cytosol of AnkG cKO mice with significant perinuclear localization (**Figures 7E to 7H**, Supplemental Figure 4). PKP2 mislocalization was exacerbated by

FIGURE 5 AnkG cKO TAC-Induced Mortality Not Associated With Tachyarrhythmias

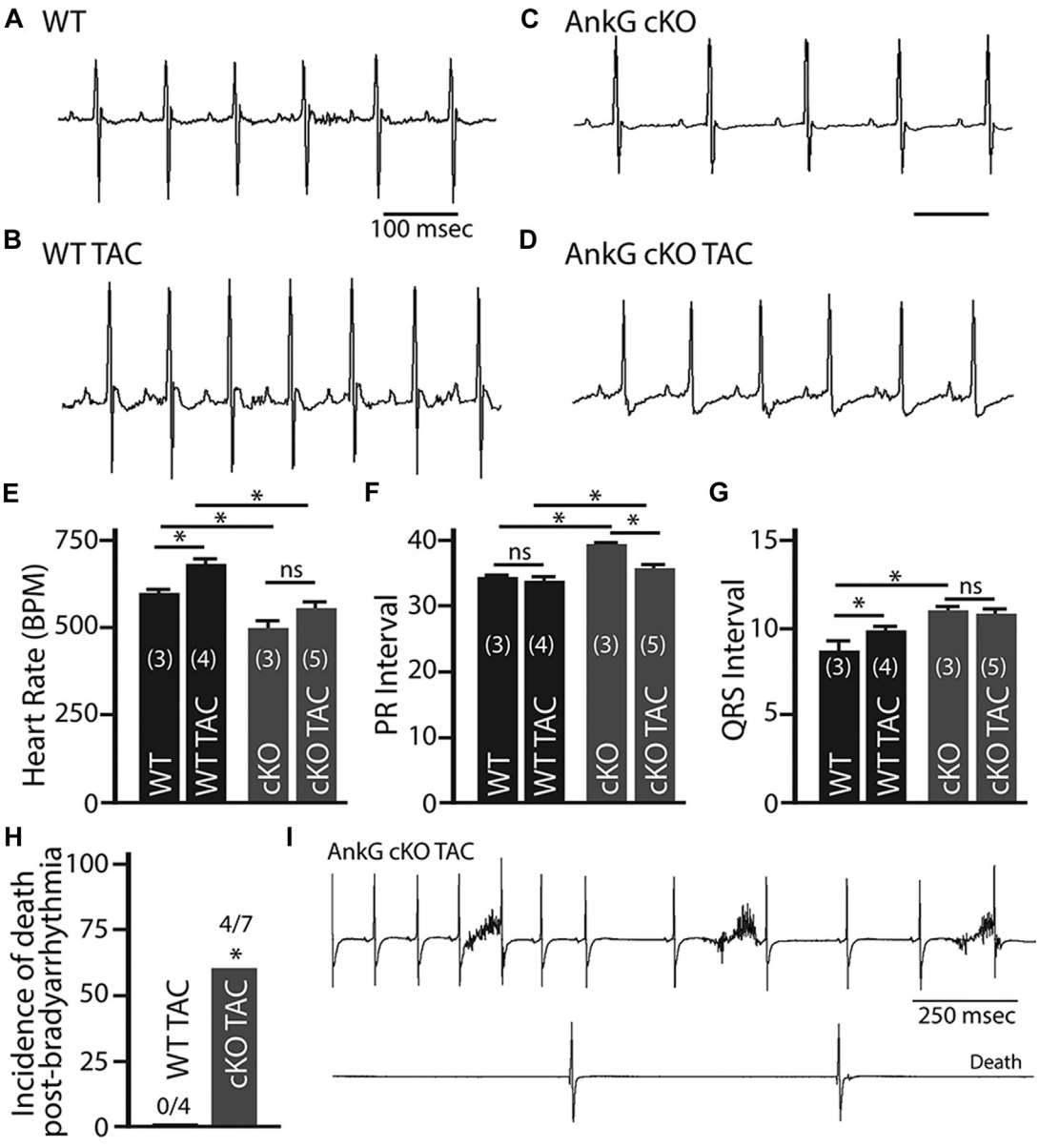

Representative ECGs from ambulatory control mice at **(A)** baseline and **(B)** 2 weeks post-TAC reveal an increase in resting heart rate in response to TAC. **(C)** ECGs from ambulatory AnkG cKO mice demonstrate decreased resting heart rate at baseline. **(D)** In response to TAC, AnkG cKO mice display decreased resting heart rate relative to wild-type controls. Scale bar = 100 ms. **(E)** Quantification of average resting heart rates in all experimental groups (n for each group listed in bar graph; $p < 0.05$). AnkG cKO mice display increased **(F)** PR interval and **(G)** QRS interval at baseline and after TAC relative to controls (n for each group listed in bar graph; $p < 0.05$). **(H)** AnkG cKO mice show an increased rate of spontaneous death. **(I)** Telemetric monitoring demonstrates that AnkG cKO animals develop severe bradycardia eventually leading to death. Scale bar = 250 ms. BPM = beats/min; other abbreviations as in Figures 2 and 3.

the 2-week TAC protocol with significant intracellular puncta in AnkG cKO mice (Figure 7H, Supplemental Figure 4). Similar results were observed in intact tissue (Supplemental Figure 5). Notably, AnkG loss did not alter all intercalated disc components (Figures 7I to 7L). For example, although N-cadherin expression was increased in response to pressure overload, we observed no defects in N-cadherin expression or

FIGURE 6 Identification of New AnkG-Associated Cellular Pathways

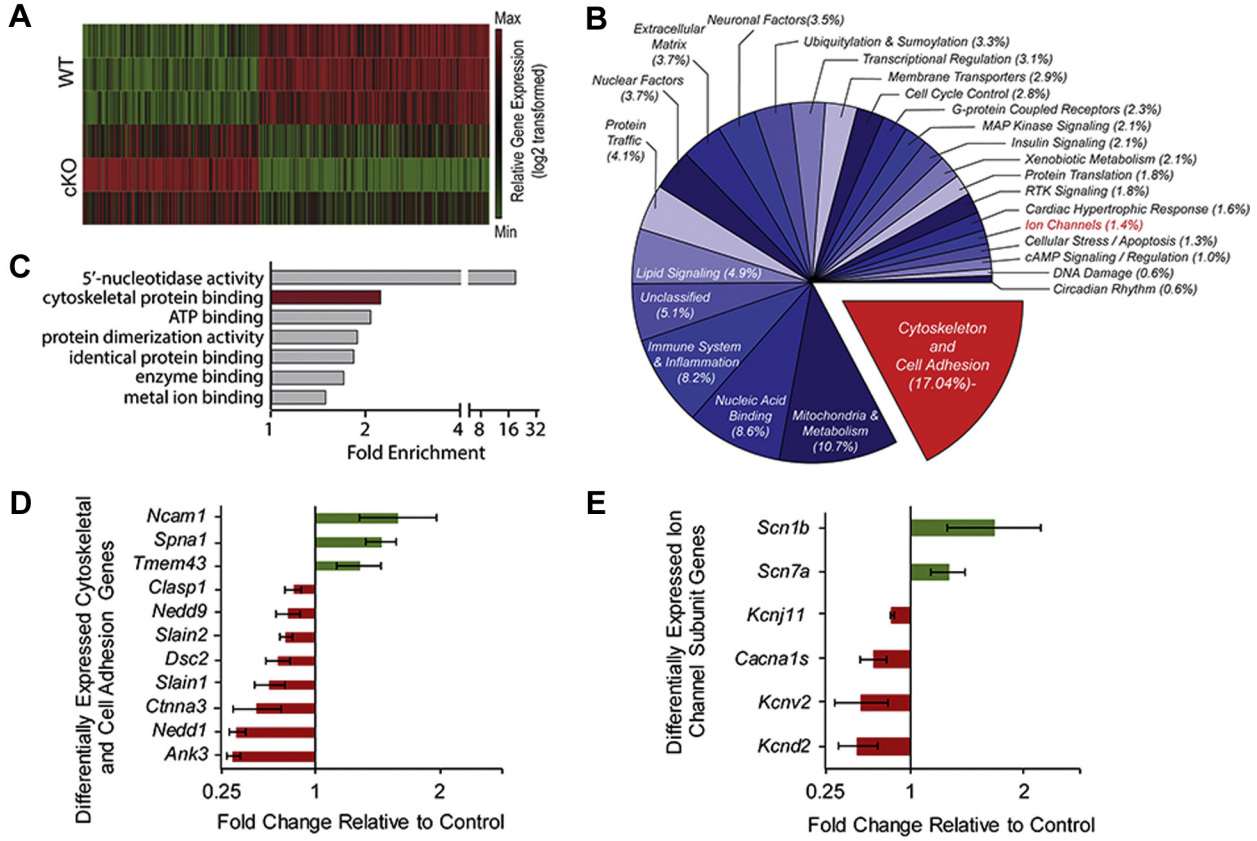

(A) Representative heat map of transcript analysis of the left ventricle of control and AnkG cKO mice. Of >25,000 transcripts analyzed, fewer than 500 displayed a significant change in expression (n = 3/genotype; $p < 0.05$). **(B and C)** Analysis of differentially expressed transcripts between control and AnkG cKO mice. Notably, 21.5% of these transcripts represent cytoskeletal, cytoskeletal-binding, and/or cell adhesion molecules. **(D)** Selective analysis of differentially expressed cytoskeletal and cell adhesion transcripts between control and AnkG cKO left ventricle. **(E)** Selective analysis of differentially expressed ion channel subunit transcripts between control and AnkG cKO left ventricle ($p < 0.05$). Abbreviations as in Figures 2 and 3.

intercalated disc localization in the absence of AnkG. Further, we observed no significant differences in the expression or localization of β-catenin, αII-spectrin, or α-tubulin between control and AnkG cKO hearts at baseline or 2 weeks post-TAC.

Finally, we examined desmin, the final downstream node for integration of the desmosome with the intermediate filament network. We observed no significant change in total desmin levels regardless of genotype or treatment condition (Supplemental Figure 6). Further, the 2-week TAC protocol produced minimal changes in desmin organization in WT mice (Supplemental Figure 6). However, in AnkG cKO hearts, we observed a significant reduction in desmin localization at the cardiac intercalated disc (Supplemental Figure 6). This loss was pronounced in the TAC animals. Thus, the loss of AnkG has a profound impact on critical cardiac regulatory proteins, including DSP, PKP2, and desmin.

AnkG HEARTS DISPLAY ALTERED EXPRESSION OF MEMBRANE ION CHANNELS. Our data support multifunctional roles of AnkG for both cardiac electrical and structural function via interaction with a host of disparate cytosolic and membrane partners. Mechanistically however, questions remain regarding the role of direct versus indirect pathways for AnkG protein partner regulation. To test the direct impact of AnkG deficiency on well-established intercalated disc membrane proteins, we evaluated AnkG in the heart at

FIGURE 7 AnkG Loss Has a Direct Impact on Myocyte Desmoplakin and PKP2 Expression

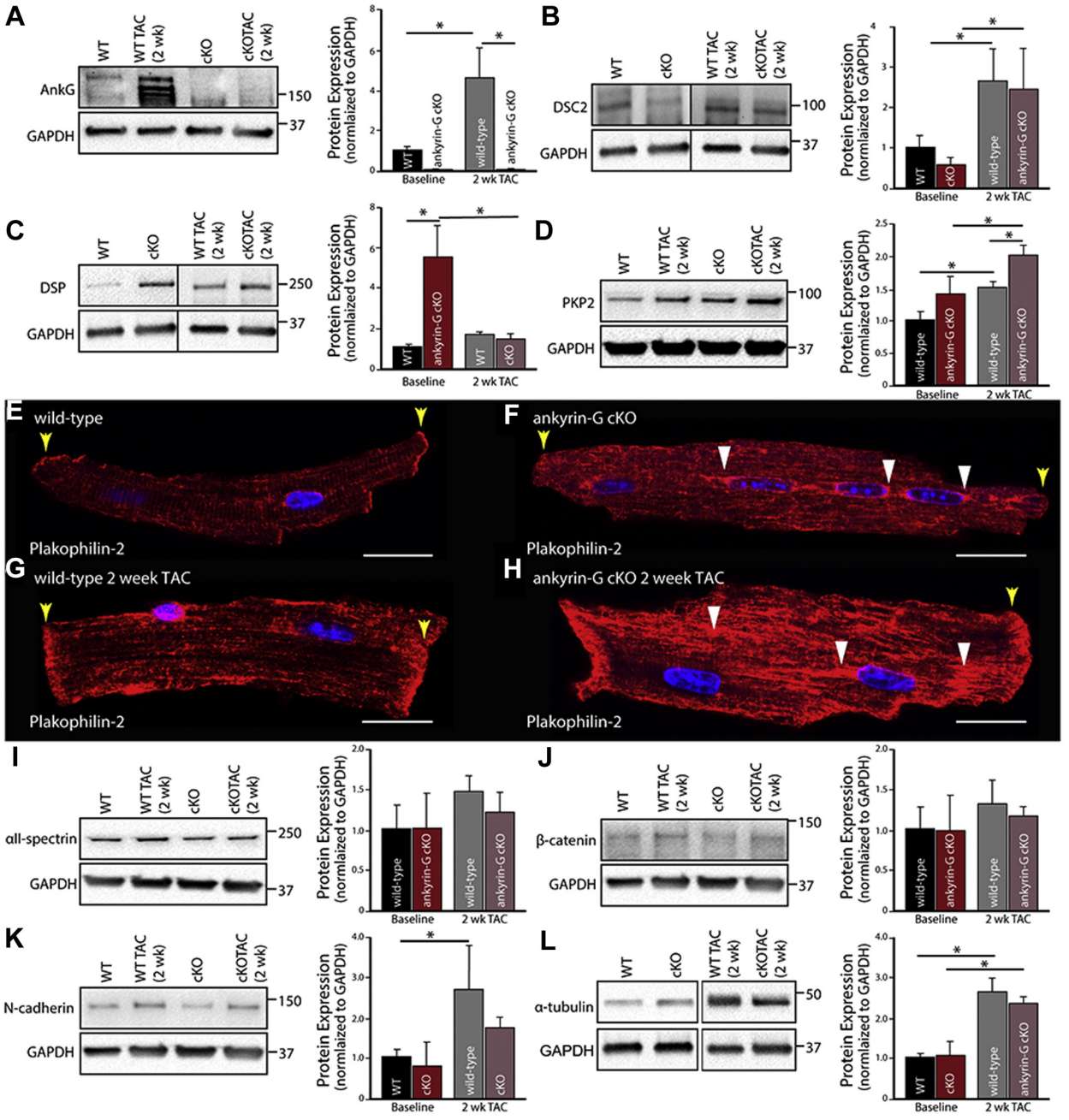

(A to D) AnkG, desmocollin-2 (DSC2), desmoplakin (DSP), and plakophilin-2 (PKP2) expression in control and AnkG cKO hearts at baseline and following 2 weeks TAC ($n = 3$; $p < 0.05$). **(E to H)** PKP2 localization in control and AnkG myocytes at baseline and following 2 weeks TAC. **Yellow arrows** denote disc, whereas **white arrowheads** denote PKP2 intracellular localization in AnkG cKO myocytes. Scale bar = 20 μm. **(I to L)** αII-spectrin (low molecular weight form), β-catenin, N-cadherin, and α-tubulin expression in control and AnkG cKO hearts at baseline and following 2 weeks TAC ($n = 3$; $p < 0.05$). In multiple cases, GAPDH is the same because blots were either cut or reprobed using unique antibodies for the primary probe. Abbreviations as in Figures 2 and 3

baseline. We observed a trend for decreased expression of $Na_v1.5$ in AnkG cKO hearts compared with control (Supplemental Figures 7A and 7B). Beyond $Na_v1.5$, AnkG expression is linked with connexin-43 (Cx43) membrane expression (22). However, at baseline, we observed no difference in either expression or localization of Cx43 in control versus AnkG cKO hearts (Supplemental Figures 7C and 7D). We therefore tested the impact of AnkG loss on Cx43 expression following 2 weeks TAC. In both control and AnkG cKO hearts, Cx43 expression was significantly decreased in the setting of increased afterload (Supplemental Figures 7C and 7D). However, whereas Cx43 localization was maintained in control hearts (Supplemental Figures 7E and 7F), we observed alterations in localization of Cx43 in AnkG cKO hearts following TAC (Supplemental Figures 7G and 7H) (no differences observed in baseline cKO hearts). Specifically, following 2 weeks post-TAC, control hearts showed homogeneous localization at the intercalated disc. By contrast, following 2 weeks post-TAC, AnkG cKO hearts displayed reduced, heterogeneous, and punctate connexin-43 intercalated disc immunostaining (Supplemental Figure 7H). Further, AnkG cKO hearts displayed significant intracellular and lateral membrane Cx43-positive puncta. In summary, our data indicate that AnkG, via both direct and indirect mechanisms, regulates both membrane, intercalated disc, and key components of the intermediate filament cytoskeleton in the heart. Our data support a direct role of AnkG in altered expression, localization, and function of $Na_v1.5$. However, as lateralization of Cx43 is often observed under decompensated conditions in both mice and humans, it is more likely that this finding is not directly linked with loss of AnkG. In summary, our findings are consistent with a model whereby loss of AnkG-dependent regulation of the intermediate filament network accelerates cardiac failure following decompensated physiological stress.

DISCUSSION

Originally identified as a key component of neuronal axon initial segments and Nodes of Ranvier (38), AnkG is a central node for regulating membrane and cytosolic protein complexes in excitable and non-excitable cells. In neurons, AnkG is essential for clustering Na_v and K channels at excitable membrane domains, whereas epithelial AnkG is necessary for lateral membrane biogenesis and localization of the Na/K ATPase (39,40). In the heart, AnkG is best known for its role in Na_v channel membrane targeting and regulation via its interaction with βIV-spectrin (17–19,32). Although more recent in vitro work from Sato et al. (20,22) has identified potential secondary roles for AnkG at cell membranes, the extent and severity of structural phenotypes in response to normal aging or acute stress were unexpected.

Our findings in mouse and human heart tissue illustrate striking alterations in AnkG expression during key phases of cardiac remodeling. Similarly, canine cardiomyocytes isolated from the border zone of a myocardial infarct also demonstrate significant increases in AnkG expression as soon as 48 h post-occlusion (21). Further, our work in AnkG cKO mice support an indispensable role for AnkG in normal physiological cardiac remodeling due to acute increases in afterload (pressure overload). In fact, in response to normal physiological aging or TAC, AnkG cKO mice demonstrate a severe HF phenotype characterized by chamber dilatation and severe systolic dysfunction, consistent with nonischemic dilated cardiomyopathy. Ultimately, this leads to increased mortality in AnkG cKO mice. We propose that the heart has evolved to increase expression of AnkG as a compensatory response necessary to increase and/or maintain mechanical coupling of cardiac myocytes during times of cardiac stress (permissive adaptive hypertrophy). In fact, on the basis of our data, we predict that AnkG is central for the stabilization of critical cellular infrastructure (βIV-spectrin, desmin, actin, PKP2, DSP) that link membrane proteins to the intermediate filament system. Further, we identified a host of transcriptional changes in AnkG cKO hearts that include multiple ion channels, channel subunits, and regulatory proteins. Although it will be important to understand the direct and indirect impact of AnkG expression in pure myocyte cultures, these data suggest a central role of AnkG in regulation of multiple cardiac pathways.

Mechanistically, we link AnkG deficiency with disrupted expression and cellular localization of PKP2 at baseline and following TAC. Following TAC, expression of both AnkG and PKP2 is increased, coupled with elevated AnkG/PKP2 localization at the intercalated disc. We propose that these events are necessary for the heart to compensate for chronic pressure overload. A functional link between AnkG and PKP2 is supported by work from Sato et al. (22). Specifically, siRNA-mediated silencing of AnkG in neonatal rat ventricular cardiac myocytes led to redistribution of PKP2 from sites of cell-cell contact. Consequently, this disruption in PKP2 localization produced functional decreases in intracellular adhesion strength (22). Beyond PKP2, AnkG cKO hearts display loss of both DSP and desmin. Desmosomal plaques are composed of the transmembrane cadherins desmoglein-2 (*DSG2*) and desmocollin-2 that

act as a "spot weld" between myocytes. PKP2 and plakoglobin (*JUP*) associate with the cytoplasmic tails of desmocollin-2/desmoglein-2. In order to provide strong, mechanical linking of adjacent cells into a functional tissue, desmosomes couple to the intermediate filament network. In the heart, desmin is the primary component of the intermediate filament network. The desmosomal protein DSP binds to desmin and scaffolds the desmin filaments to PKP2 and plakoglobin in the desmosome. Thus, we hypothesize that aberrant PKP2 targeting in AnkG cKO animals alters desmin localization, further weakening the cytoarchitecture in the AnkG cKO heart. Taken together, our data demonstrate a critical regulatory role for AnkG in the regulation of multiple desmosomal components at baseline and during physiological and pathological stress.

Prior investigations support a structural requirement for AnkG in multiple cell types. In neurons, AnkG is required for the stability of structural components of the axon initial segment including neurofascin-186 and neuronal cell adhesion molecule (41). Further, expression of AnkG in neurons and oligodendrocytes is responsible for the rapid structural formation of nodes of Ranvier (42). Multiple reports have demonstrated that AnkG is necessary for the retention of E-cadherin, a molecular event necessary for the biogenesis of the lateral membrane in epithelial cells (40,43). Given the presence of such severe dysfunction, however, we hypothesized that the phenotypes displayed by the AnkG cKO mice following TAC are likely caused by multiple changes to the cardiac myocyte structural components.

CONCLUSIONS

In summary, we propose that AnkG is a nodal protein required for cardiac myofilament integration with the intercalated disc, where AnkG loss results in a cascade of negative downstream molecular phenotypes including abnormal PKP2, DSP, desmin, and $Na_v1.5$. In summary, our in vivo experiments demonstrate that AnkG plays an unexpected, but necessary, role in compensatory physiologic remodeling in response to myocardial stress and implicate disruption of AnkG in the development and progression of human HF.

ADDRESS FOR CORRESPONDENCE: Dr. Peter Mohler, The Ohio State University Wexner Medical Center, The Dorothy M. Davis Heart & Lung Research Institute, 473 West 12th Avenue, Columbus, Ohio 43210. E-mail: peter.mohler@osumc.edu.

PERSPECTIVES

COMPETENCY IN MEDICAL KNOWLEDGE: Human heart failure is a complex and multifactorial process having an impact on nearly five million individuals in the United States alone. The control of normal left ventricular systolic function necessitates coordinated transmission of action potentials between heart cells and appropriate force transmission across the heart. Thus, heart cells have evolved complex molecular machinery to regulate both mechanical and electrical activity at baseline and in response to physiological and pathological stress. Development of diagnostic and treatment strategies for human heart failure are actively focused on pathways that have an impact on both electrical and structural pathways in cardiac myocytes.

TRANSLATIONAL OUTLOOK: Ankyrin proteins are expressed in both excitable and non-excitable cell types where they play critical roles in the targeting of key structural, membrane, and signaling proteins. The role of ankyrins in human physiology is clearly illustrated by the impact of human loss-of-function gene variants or animal models lacking ankyrin expression on vertebrate physiology. Ankyrin-G although previously linked with regulation of cardiac electrical activity via the regulation of cardiac ion channels is now linked with new roles in regulation of cardiac cell structural pathways. Future studies will investigate the impact of AnkG pathways on cardiac structural and electrical remodeling in human disease as well as defining modalities to stabilize AnkG activity in disease with the goal of reducing the burden of both heart failure and arrhythmia in patients.

REFERENCES

1. Sjostrand FS, Andersson E. Electron microscopy of the intercalated discs of cardiac muscle tissue. Experientia 1954;10:369–70.

2. Severs NJ. The cardiac gap junction and intercalated disc. Int J Cardiol 1990;26:137–73.

3. Li J, Patel VV, Radice GL. Dysregulation of cell adhesion proteins and cardiac arrhythmogenesis. Clin Med Res 2006;4:42–52.

4. Saffitz JE. The pathobiology of arrhythmogenic cardiomyopathy. Annu Rev Pathol 2011;6:299–321.

5. Barker RJ, Price RL, Gourdie RG. Increased association of ZO-1 with connexin43 during remodeling of cardiac gap junctions. Circ Res 2002;90:317–24.

6. Cunha SR, Hund TJ, Hashemi S, et al. Defects in ankyrin-based membrane protein targeting

pathways underlie atrial fibrillation. Circulation 2011;124:1212–22.

7. Hund TJ, Wright PJ, Dun W, Snyder JS, Boyden PA, Mohler PJ. Regulation of the ankyrin-B-based targeting pathway following myocardial infarction. Cardiovasc Res 2009;81:742–9.

8. Kashef F, Li J, Wright P, et al. Ankyrin-B protein in heart failure: identification of a new component of metazoan cardioprotection. J Biol Chem 2012; 287:30268–81.

9. Le Scouarnec S, Bhasin N, Vieyres C, et al. Dysfunction in ankyrin-B-dependent ion channel and transporter targeting causes human sinus node disease. Proc Natl Acad Sci U S A 2008;105:15617–22.

10. Mohler PJ, Le Scouarnec S, Denjoy I, et al. Defining the cellular phenotype of "ankyrin-B syndrome" variants: human ANK2 variants associated with clinical phenotypes display a spectrum of activities in cardiomyocytes. Circulation 2007; 115:432–41.

11. Mohler PJ, Schott JJ, Gramolini AO, et al. Ankyrin-B mutation causes type 4 long-QT cardiac arrhythmia and sudden cardiac death. Nature 2003;421:634–9.

12. Mohler PJ, Splawski I, Napolitano C, et al. A cardiac arrhythmia syndrome caused by loss of ankyrin-B function. Proc Natl Acad Sci U S A 2004; 101:9137–42.

13. Sedlacek K, Stark K, Cunha SR, et al. Common genetic variants in ANK2 modulate QT interval: results from the KORA study. Circ Cardiovasc Genet 2008;1:93–9.

14. Musa H, Murphy NP, Curran J, et al. Common human ANK2 variant confers in vivo arrhythmia phenotypes. Heart Rhythm 2016;13:1932–40.

15. Swayne LA, Murphy NP, Asuri S, et al. Novel variant in the ANK2 membrane-binding domain is associated with ankyrin-B syndrome and structural heart disease in a First Nations population with a high rate of long QT syndrome. Circ Cardiovasc Genet 2017;10:e001537.

16. Huq AJ, Pertile MD, Davis AM, et al. A Novel mechanism for human cardiac ankyrin-B syndrome due to reciprocal chromosomal translocation. Heart Lung Circ 2017;26:612–8.

17. Mohler PJ, Rivolta I, Napolitano C, et al. Nav1.5 E1053K mutation causing Brugada syndrome blocks binding to ankyrin-G and expression of Nav1.5 on the surface of cardiomyocytes. Proc Natl Acad Sci U S A 2004;101:17533–8.

18. Makara MA, Curran J, Little SC, et al. Ankyrin-G coordinates intercalated disc signaling platform to regulate cardiac excitability in vivo. Circ Res 2014; 115:929–38.

19. Lowe JS, Palygin O, Bhasin N, et al. Voltage-gated Nav channel targeting in the heart requires an ankyrin-G dependent cellular pathway. J Cell Biol 2008;180:173–86.

20. Sato PY, Musa H, Coombs W, et al. Loss of plakophilin-2 expression leads to decreased sodium current and slower conduction velocity in cultured cardiac myocytes. Circ Res 2009;105:523–6.

21. Dun W, Lowe JS, Wright P, Hund TJ, Mohler PJ, Boyden PA. Ankyrin-G participates in INa remodeling in myocytes from the border zones of infarcted canine heart. PLoS One 2013;8:e78087.

22. Sato PY, Coombs W, Lin X, et al. Interactions between ankyrin-G, Plakophilin-2, and Connexin43 at the cardiac intercalated disc. Circ Res 2011;109:193–201.

23. Gudmundsson H, Hund TJ, Wright PJ, et al. EH domain proteins regulate cardiac membrane protein targeting. Circ Res 2010;107:84–95.

24. Kline CF, Kurata HT, Hund TJ, et al. Dual role of K ATP channel C-terminal motif in membrane targeting and metabolic regulation. Proc Natl Acad Sci U S A 2009;106:16669–74.

25. Cunha SR, Bhasin N, Mohler PJ. Targeting and stability of Na/Ca exchanger 1 in cardiomyocytes requires direct interaction with the membrane adaptor ankyrin-B. J Biol Chem 2007;282: 4875–83.

26. Makara MA, Hoang KV, Ganesan LP, et al. Cardiac electrical and structural changes during bacterial infection: an instructive model to study cardiac dysfunction in sepsis. J Am Heart Assoc 2016;5:e00382.

27. Doctor RB, Bennett V, Mandel LJ. Degradation of spectrin and ankyrin in the ischemic rat kidney. Am J Physiol 1993;264:C1003–13.

28. Schafer DP, Jha S, Liu F, Akella T, McCullough LD, Rasband MN. Disruption of the axon initial segment cytoskeleton is a new mechanism for neuronal injury. J Neurosci 2009;29:13242–54.

29. Furihata T, Kinugawa S, Takada S, et al. The experimental model of transition from compensated cardiac hypertrophy to failure created by transverse aortic constriction in mice. Int J Cardiol Heart Vasc 2016;11:24–8.

30. Tachibana H, Perrino C, Takaoka H, Davis RJ, Naga Prasad SV, Rockman HA. JNK1 is required to preserve cardiac function in the early response to pressure overload. Biochem Biophys Res Commun 2006;343:1060–6.

31. Ling H, Zhang T, Pereira L, et al. Requirement for Ca2+/calmodulin-dependent kinase II in the transition from pressure overload-induced cardiac hypertrophy to heart failure in mice. J Clin Invest 2009;119:1230–40.

32. Hund TJ, Koval OM, Li J, et al. A beta(IV)-spectrin/CaMKII signaling complex is essential for membrane excitability in mice. J Clin Invest 2010; 120:3508–19.

33. Chkourko HS, Guerrero-Serna G, Lin X, et al. Remodeling of mechanical junctions and of microtubule-associated proteins accompany cardiac connexin43 lateralization. Heart Rhythm 2012;9:1133–40.e6.

34. Saito T, Asai K, Sato S, et al. Autophagic vacuoles in cardiomyocytes of dilated cardiomyopathy with initially decompensated heart failure predict improved prognosis. Autophagy 2016;12:579–87.

35. Xu X, Pacheco BD, Leng L, Bucala R, Ren J. Macrophage migration inhibitory factor plays a permissive role in the maintenance of cardiac contractile function under starvation through regulation of autophagy. Cardiovasc Res 2013;99: 412–21.

36. Royer A, van Veen TA, Le Bouter S, et al. Mouse model of SCN5A-linked hereditary Lenegre's disease: age-related conduction slowing and myocardial fibrosis. Circulation 2005;111:1738–46.

37. Leoni AL, Gavillet B, Rougier JS, et al. Variable Na(v)1.5 protein expression from the wild-type allele correlates with the penetrance of cardiac conduction disease in the Scn5a mouse model. PLoS One 2010;5:e9298.

38. Kordeli E, Lambert S, Bennett V. AnkyrinG. A new ankyrin gene with neural-specific isoforms localized at the axonal initial segment and node of Ranvier. J Biol Chem 1995;270:2352–9.

39. Yoshimura T, Rasband MN. Axon initial segments: diverse and dynamic neuronal compartments. Curr Opin Neurobiol 2014;27:96–102.

40. Kizhatil K, Bennett V. Lateral membrane biogenesis in human bronchial epithelial cells requires 190-kDa ankyrin-G. J Biol Chem 2004;279: 16706–14.

41. Jenkins SM, Bennett V. Ankyrin-G coordinates assembly of the spectrin-based membrane skeleton, voltage-gated sodium channels, and L1 CAMs at Purkinje neuron initial segments. J Cell Biol 2001;155:739–46.

42. Chang KJ, Zollinger DR, Susuki K, et al. Glial ankyrins facilitate paranodal axoglial junction assembly. Nat Neurosci 2014;17:1673–81.

43. Kizhatil K, Yoon W, Mohler PJ, Davis LH, Hoffman JA, Bennett V. Ankyrin-G and beta2-spectrin collaborate in biogenesis of lateral membrane of human bronchial epithelial cells. J Biol Chem 2007;282:2029–37.

KEY WORDS ankyrin, arrhythmia, cytoskeleton, heart failure, ion channel, $Na_v1.5$

APPENDIX For supplemental figures and tables, please see the online version of this paper.